IEEE Access
Multidisciplinary | Rapid Review | Open Access Journal

Received February 12, 2020, accepted February 22, 2020, date of publication March 2, 2020, date of current version March 12, 2020.

*Digital Object Identifier 10.1109/ACCESS.2020.2977395*

# Adaptive Sliding Mode Control With Feedforward Compensator for Energy-Efficient and High-Speed Precision Motion of Feed Drive Systems

**MATHEW RENNY MSUKWA[1,2], (Student Member, IEEE), ENOCK WILLIAM NSHAMA[1,3], AND NAOKI UCHIYAMA[1], (Member, IEEE)**

[1]Department of Mechanical Engineering, Toyohashi University of Technology, Toyohashi 441-8580, Japan
[2]Department of Electrical Engineering, University of Dar es Salaam, Dar es Salaam 35091, Tanzania
[3]Department of Mechanical Engineering, University of Dar es Salaam, Dar es Salaam 35091, Tanzania

Corresponding author: Naoki Uchiyama (uchiyama@tut.jp)

This work was supported in part by the Machine Tool Technologies Research Foundation, San Francisco, USA, and in part by the Magnescale Co., Ltd., Kanagawa, Japan.

**ABSTRACT** Industrial feed drive systems, particularly ball-screw and lead-screw feed drives are among the dominating components in production and manufacturing industries. They operate around the clock and at high speeds for coping with the growing production demands. Adversely, high-speed motions cause mechanical vibration, high-energy consumption, and poor tracking performance. Thus, over the years, the research community has invested in precision control and energy saving for these systems. Although there are many control strategies in the literature, such as sliding mode and model predictive controls, further research is necessary for performance enhancement. This study focuses on both high-speed precision control and energy-saving control for feed drive systems. An adaptive nonlinear sliding mode controller with a feedforward compensator for plant uncertainties is designed and its stability is confirmed through the Lyapunov stability theories. For performance evaluation, simulations and experiments are conducted and results are compared with those of an adaptive nonlinear sliding model controller. Results revealed that, based on the proposed controller, the tracking errors of feed drive systems can be reduced by about 33% on average and the maximum tracking error by about 64% on average. In addition, the energy consumption can be reduced by about 2% under similar tracking performance.

**INDEX TERMS** Computer numerical controlled machines, controller design, adaptive control, sliding mode control, machine tools, nonlinear control, uncertainty dynamics.

## I. INTRODUCTION

Feed drive systems are among the dominating motion components in production and manufacturing industries owing to their wide range of use, for instance in multi-axis motions [1]–[5]. The growing demand for precise products poses a need for high-speed production systems with higher accuracy. In addition, because in most cases, feed drive systems operate around the clock, they are among the major consumers of the industrial energy supply. Thus, energy consumption is part of the reasons for using lighter components in feed drive systems. While high-speed motion is preferred, it causes vibration in light systems, high-energy consumption, and poor tracking performance. As explained in [3], [6], [7], the control performance depends greatly on the systems' vibration, un-modeled uncertainties and external disturbances.

Many researches have been focusing on positioning and tracking control of servomotors, which are widely used in motion control applications owing to their basic advantages, such as high power-density and torque to inertia ratio, high performance and efficiency and low noise [8], [9]. On doing so, classical and modern control techniques such as sliding mode control (SMC), adaptive control, dynamic friction compensation methods, back-stepping control have been widely applied [8], [10]–[14]. On the other hand, for applications such as in feed drive systems, repetitive and iterative learning controls are commonly used under the assumption that these

The associate editor coordinating the review of this manuscript and approving it for publication was Zheng Chen.


This work is licensed under a Creative Commons Attribution 4.0 License. For more information, see http://creativecommons.org/licenses/by/4.0/

systems are used for mass-productions [3]. However, since there are many feed drive applications that are not repetitive, it is indispensable to consider control strategies for general applications.

In [15], a practical method called robust integral of the sign of the error controller is employed and synthesize with a continuous differentiable friction model in order to achieve high accuracy motion of a dc motor. In the controller, a model based desired compensation is employed so as to reduce control chattering and sensitivity to noise during application, and hence tracking performance can be enhanced.

Recently, linear motors are being applied increasingly in high speed machine tools. However, they are more expensive and sensitive to disturbance because of the direct conversion of motor current to driving force without a motion transmission gear. They also face synchronization problem in practical applications. Research work in [16] and [17] have proposed an effective methods for eliminating the synchronization problem. On the other hand, ball-screw feed drives are often used in machine tools because of advantages in relation to low costs, high stiffness against cutting forces, and robustness to disturbances and table load variations due to their high gear ratio. In addition, some machining tasks require high cutting forces, consistency, and stability, and hence a ball-screw drive is the best solution. Therefore, we believe that it is inevitable to continue conducting research on ball-screw feed drive systems.

Robust controllers such as SMC have proven to provide reasonable performance under the effect of external disturbance and system uncertainties [6], [18]–[23]. The SMC, apart from its simplicity in design, it is robust against perturbation and invariant to matched uncertainties. Other variants of the SMC includes adaptive sliding mode control (ASMC) and nonlinear sliding mode control. They are more flexible and offer higher tracking performance compared to the traditional SMC [24], [25].

On the other hand, model-based approaches such as feedforward friction compensator are applied to cancel out the effect of the estimated friction force. However, because friction sources are generally of complex nonlinear properties, it is difficult to find a perfect model and the performance depends exclusively on the veracity of the estimated model [26], [27]. In [28], continuously differentiable nonlinear friction model is derived by modifying LuGre model which is piecewise continuous, and then propose a controller to take care of parametric uncertainties along with nonlinear friction compensation. Despite the promising performance of the mentioned approaches, it is indispensable to enhance both the tracking performance and energy consumption of feed drive systems.

Generally, feed drive systems include various nonlinear uncertainties like backlash, friction forces, modelling errors, parameter variation etc,. In ball screw feed drive systems, preloading is applied. It can be described as the tension induced on the ball screw drive when no external loads are applied. The purpose of the additional load is to eliminate backlash and also increase position accuracy of the ball screw during operation [29]. Therefore, because of preloading, backlash is not a big problem in ball screw drive systems but friction is the main disturbance. Some research work focused on control of a specific type of uncertainty. For example, [30] proposed a joint toque control for backlash compensation in two-inertia system where backlash is modelled as a dead zone. However, for completely cancellation of specific uncertainties, it requires having their accurate models. In practice, modelling each of the uncertainty which may exist in a plant is impractical. Therefore, it is inevitable to design a controller which is robust and can automatically cancel out the effect of these uncertainties without focusing on its specific type.

The primary objective of this paper is to improve the tracking performance by explicitly considering the uncertainty dynamics. A nonlinear SMC with a feedforward compensator for system uncertainties is applied. As proposed in [31], the feedforward compensator refers to the modeled system with assumed uncertainty dynamics and the controller is designed by taking the difference between a reference model and the real system. The proposed method enhances the tracking performance of feed drive systems while maintaining the required energy. An addition of another compensator for a specific uncertainty is expected not to degrade the performance of the proposed controller but enhance it. Through Lyapunov stability theory, the system stability was analyzed and confirmed and its convergence to the sliding surface was assured.

The rest of this article is organized as follows: Section II presents the system dynamics of a typical feed drive system followed by controller design and stability analysis section III. Section IV describes the methodology for energy consumption in feed drive systems. Simulation and experimental analyses are presented in section V followed by concluding remarks in section VII.

## II. DYNAMICS MODEL OF X-Y TABLE

Because feed drive systems are of many configurations, a typical biaxial setup, also referred to as X-Y table, is considered in this article. Its dynamics can be represented in a decoupled format as follows [32]:

$$\begin{aligned} &M\ddot{x} + C\dot{x} + L\text{sign}(\dot{x}) + d = f, \\ &M = \text{diag}\,(m_i), \quad C = \text{diag}\,(c_i), \quad L = \text{diag}\,(l_i), \quad i = \{1, 2\}, \\ &f = [f_1,\ f_2]^T, \quad d = [d_1,\ d_2]^T, \quad x = [x_1,\ x_2]^T, \end{aligned} \tag{1}$$

whereas $m_i$, $c_i$, and $l_i$ represent the mass, viscous friction coefficient, and Coulomb friction force for each drive axis $i$, respectively. The input (driving force), external disturbance and position of each drive axis are respectively denoted as $f_i, d_i$, and $x_i$. Noting that the drive axes are driven by servo motors that are mechanically coupled to the system, the dynamics of these motors are included to the system. The dynamics of the attached motors is defined as

follows [24]:

$$N\ddot{\theta} + H\dot{\theta} + \tau = K_t i_a,$$
$$N = \text{diag}\,(n_i)\,, \quad H = \text{diag}\,(h_i)\,, \; K_t = \text{diag}\left(k_{t_i}\right),$$
$$\theta = [\theta_1,\ \theta_2]^T\,, \quad \tau = [\tau_1,\ \tau_2]^T\,, \; i_a = \left[i_{a_1}, i_{a_2}\right]^T\,, \quad (2)$$

with $n_i$, $\theta_i$, $h_i$, $\tau_i$, $k_{ti}$ and $i_{ai}$ being the inertia, angular position, viscous friction coefficient, output torque, torque constant, and the input electric current for each motor $i$, respectively.

Therefore, the plant dynamics can be represented as

$$u = J_e\ddot{x} + B_e\dot{x} + L\text{sign}(\dot{x}) + d,$$
$$J_e = \text{diag}\left(\frac{4\pi^2\, n_i + m_i p_i^2}{p_i^2}\right),$$
$$B_e = \text{diag}\left(\frac{4\pi^2\, h_i + c_i p_i^2}{p_i^2}\right),$$
$$u = K_\mu i_a,\ K_\mu = \text{diag}\left(\frac{2\pi\, k_{t_i}}{p_i}\right), \quad (3)$$

where $p$ refers to the pitch of ball-screws that converts the motors' angular motion to the linear motion of the drive axes. The nominal values of $J_e$ and $B_e$ are assumed to be known.

## III. CONTROLLER DESIGN

Prior to the controller design, we define the positional tracking error of the system as follows:

$$e = x_r - x,$$
$$e = [e_1,\ e_2]^T,\ x_r = [x_{r_1},\ x_{r_2}]^T, \quad (4)$$

where $x_r$ is the reference position. From (3), the error dynamics can be written as

$$\ddot{e} = \ddot{x}_r - J_e^{-1}\left\{u - B_e\dot{x} - L\text{sign}(\dot{x}) - d\right\}. \quad (5)$$

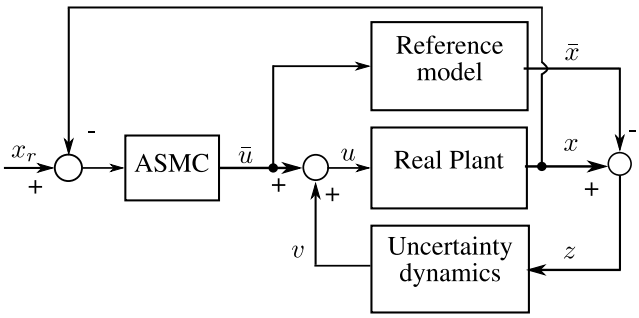


**FIGURE 1.** Block diagram of the proposed control system.

The proposed control structure comprises of the reference plant model, real plant, and the uncertainty dynamics compensator as shown in the block diagram (Fig. 1). The following linear equation is considered as the reference model:

$$\bar{u} = J_e\ddot{\bar{x}} + B_e\dot{\bar{x}}, \quad \bar{x} = [\bar{x}_1,\ \bar{x}_2]^T \quad (6)$$

where $\bar{x}_i$ and $\bar{u}$ are the position of the $i^{th}$ drive axis and the input vector to the reference model, respectively. The control input to the real plant is defined as $u = \bar{u} + v$, where $v$ is the compensator for the uncertainty dynamics.

### A. SLIDING MODE CONTROLLER DESIGN

To design a sliding mode controller, we first considered selection of a nonlinear sliding surface that will ensure that the system can effectively track the reference trajectory. The sliding surface has to guarantee that the control systems asymptotically stable. Then, a control law is selected so as to drive the system to follow the reference trajectory. To confirm that the control system is stable, the selected control law has to ensure that the error dynamics is exponentially decaying with time.

#### 1) NONLINEAR SLIDING SURFACE DESIGN

The response of a dynamic system depends sorely on its damping ratio [33]. As shown in Fig. 2, if the damping ratio is high (a), the system response becomes slow with large tracking error. On the contrary, if the damping ration is too small (b), the response becomes too fast with large overshoots. The overshoots causes poor tracking performance and leads to excessive energy consumption. It is desirable to have a system that can respond as fast as possible yet without overshoots. For doing that, a variable damping ratio is applied such that at a low damping ratio is applied at the initial stage to assist fast response and gradually increased to minimize overshoots. A variable damping ratio allows for better tracking performance while minimizing the energy consumption.

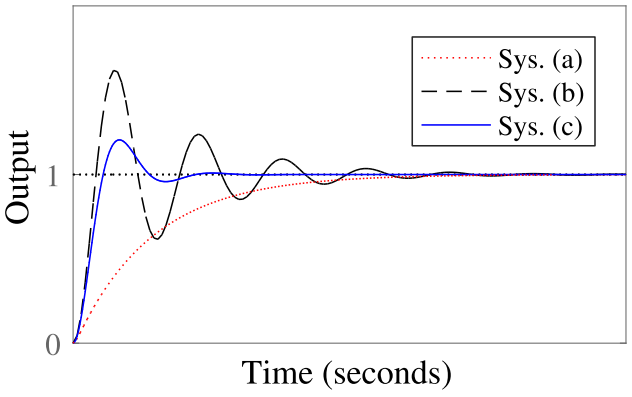


**FIGURE 2.** System response with different damping ratio. System (a) with high damping ratio, System (b) with low damping ratio, System (c) with nonlinear damping ratio [25].

In this study, the following nonlinear sliding surface is applied [34]:

$$\bar{s} = \begin{bmatrix} A & I \end{bmatrix} \begin{bmatrix} e \\ \dot{e} \end{bmatrix},$$
$$A = \text{diag}(\lambda_i + \psi_i\gamma_i). \quad (7)$$

where $\lambda_i$ is the linear term of the sliding surface. The linear term is selected by ensuring that predominant poles have small damping ratio. $\gamma_i$ is a positive linear term that assist on adjusting the damping ratio. $\psi_i$ is a non-negative differentiable nonlinear function of the error, which is upper bounded such that $\psi_i \leq \psi_{max_i}$ and its role is to facilitate on adjusting

the damping ratio of the system and it changes the damping ratio of the system. As the the system output varies from its initial value, $\psi_i$ gradually increases the damping ratio. Based on the nonlinear function presented in [35] for a step-type reference trajectory, The following $\psi_i$ is considered in this study:

$$\psi_i = \beta_i \frac{\exp\left(-\bar{k}_i \tilde{e}_i\right) + \exp\left(\bar{k}_i \tilde{e}_i\right)}{2}$$
$$\tilde{e}_i = \begin{cases} e_i & |e_i| \le e_{max_i} \\ e_{max_i} \text{sign}\left(e_i\right) & |e_i| > e_{max_i} \end{cases} \tag{8}$$

where $\beta_i$, $\bar{k}_i$ and $e_{max_i}$ are the positive tuning parameters defined by the user. $\beta_i$ and $\bar{k}_i$ determine the final damping ratio and the variation rate of the nonlinear function $\psi_i$, respectively. If the system output is far from the desired value, the magnitude of $\psi_i$ becomes small, this provides a low damping ratio and speeds up the system response. On the sliding surface, $\bar{s} = 0$, we have

$$\dot{e} = -Ae, \tag{9}$$

where $A$ is not a constant matrix. To verify the stability of the sliding surface $\dot{\bar{s}} = 0$, the following Lyapunov function is considered:

$$V = \frac{1}{2} e^T e \tag{10}$$

Substituting (9) into the time derivative of $V$ leads to

$$\dot{V} = -e^T A e. \tag{11}$$

Since $A$ is a positive definite matrix, the asymptotic stability is guaranteed.

#### 2) SELECTION OF CONTROL LAW

The control law is designed such that, from any initial condition, the trajectory of the reference model is attracted towards the sliding surface. Based on the proposed sliding surface and the feed drive dynamics, the following control law is designed:

$$\bar{u} = J_e \left(\ddot{x}_r + A\dot{e} + \hat{K}\bar{s} + Be\right) + B_e \dot{x} + L\text{sign}\left(\dot{x}\right),$$
$$B = \text{diag}\left(\dot{\psi}_i \gamma_i\right), \quad \hat{K} = \text{diag}\left(\hat{k}_i\right), \tag{12}$$

where $\hat{k}_i$ is the adaptive gain. Only typical friction compensation is considered because of difficulty in identification and adaption and uncertainty dynamics compensation of other small disturbances. The adaptive law is chosen based on the idea in [36] as follows:

$$\dot{\hat{k}}_i = \begin{cases} \xi_i |\bar{s}_i| \text{sign}(|\bar{s}_i| - \varepsilon_i) & \text{if } \hat{k}_i > \varpi_i \\ \zeta_i & \text{otherwise} \end{cases} \tag{13}$$

where $\varepsilon_i$, $\varpi_i$, $\zeta_i$, and $\xi_i$ are positive constants. The parameter $\zeta_i$ is introduced in order to obtain positive values for $\hat{k}_i$. After the sliding mode with respect to $\bar{s}_i$ is established, the gain adaption law (13) allows the gain $\hat{k}_i$ to decrease while $|\bar{s}_i| < \varepsilon_i$. This means gain $\hat{k}_i$ will remain at the smallest level while satisfying the required accuracy of $\bar{s}_i$.

### B. UNCERTAINTY COMPENSATION

Since the real system can be different from the approximated reference model, a controller is designed to compensate for the resulting uncertainty, which is eventually the difference between the real system and the referred model. The uncertainty states are defined as

$$\begin{bmatrix} z_i \\ \dot{z}_i \end{bmatrix} = \begin{bmatrix} x_i \\ \dot{x}_i \end{bmatrix} - \begin{bmatrix} \bar{x}_i \\ \dot{\bar{x}}_i \end{bmatrix}, \tag{14}$$

where $z_i$ is the measurable output of the uncertainty dynamics. $x$ and $\bar{x}$ are the actual positions of the real system and the reference model, respectively.

The uncertainty dynamics is assumed as a second order nonlinear dynamics [31]:

$$\ddot{z}_i = q_i\left(z\right) + v_i, \tag{15}$$

where $v_i$ is the control input signal of the uncertainty dynamics, and $q_i\left(z\right)$ is the unknown time-varying dynamics of the system. $q_i\left(z\right)$ is assumed to be upper bounded by $Q_i$ as

$$|q_i| \le Q_i. \tag{16}$$

The tracking error for the uncertainty dynamics is described as follows:

$$\tilde{z}_i = z_i - z_{r_i} \tag{17}$$

where $\tilde{z}_i$ is the tracking error and $z_{r_i}$ is the desired position of the uncertainty dynamics. The aim of the the control structure is to converge the output of uncertainty dynamics to zero. Therefore, the desired value for the uncertainty position, velocity, and acceleration are set to zero.

To track the desired position, a linear SMC is used to cancel the uncertainties. The following sliding surface that consists of the uncertainty error and the uncertainty error rate is used

$$s_i = \alpha_i \tilde{z}_i + \dot{\tilde{z}}_i, \tag{18}$$

where $\alpha_i$ is the positive constant.

The rate of the sliding surface is obtained by taking the time derivative of the sliding surface in (18) as follows:

$$\begin{aligned} \dot{s}_i &= \alpha_i \dot{\tilde{z}}_i + \ddot{\tilde{z}}_i \\ &= \alpha_i \dot{\tilde{z}}_i + \ddot{z}_i - \ddot{z}_{r_i} \\ &= q_i(z) + v_i - \ddot{z}_{r_i} + \alpha_i \dot{\tilde{z}}_i. \end{aligned} \tag{19}$$

To achieve $\dot{s}_i = 0$ for the stable sliding surface, the following control law $v_i$ is used [31].

$$v_i = \ddot{z}_{r_i} - \alpha_i \dot{\tilde{z}}_i - \mu_i \text{sign}\left(s_i\right) - 2\mu_i \frac{s_i}{|s_i|}. \tag{20}$$

The function $q_i$ is unknown, therefore the control law must not contain the function $q_i$. Instead, the term $\mu_i \text{sign}\left(s_i\right)$ is added to ensure $\dot{s} = 0$. Here $\mu_i$ is a positive adaptive gain, and is chosen as

$$\dot{\mu}_i = \rho_i |s_i|, \tag{21}$$

where $\rho_i$ is a positive constant.

*Property:* The control algorithm ($u_i = \bar{u}_i + v_i$) consists of the sliding mode controller based on the uncertainty dynamics and the nonlinear sliding mode controller as illustrated in Fig. 1.

Because the switching function, *sign* causes chattering a phenomenon in control systems, during implementation, when $|s_i| \leq \delta_i$, the *sign* function in (20) is replaced by the following equation which is typical in the previous works [31].

$$\text{sign}(s_i) \simeq \frac{s_i}{|s_i| + \delta_i}, \tag{22}$$

In addition, if the function $q_i$ is upper bounded by $Q_i$ as in (16), and the final value of the controller gain $\mu_i^*$ in (20) is such that $\mu_i^* > Q_i$, then $z_i$ converges asymptotically to zero and sliding motion is achieved.

*Proof:* The following Lyapunov function candidate is considered:

$$V_i = \frac{1}{2}\bar{s}_i^2 + \frac{1}{2}s_i^2 + \frac{1}{2\rho_i}\left(\mu_i - \mu_i^*\right)^2. \tag{23}$$

The time derivative of (23) is given by:

$$\dot{V}_i = \bar{s}_i\dot{\bar{s}}_i + s_i\dot{s}_i + \frac{\dot{\mu}_i}{\rho_i}\left(\mu_i - \mu_i^*\right). \tag{24}$$

From the time derivative of (7) and (18), (24) becomes

$$\dot{V}_i = \bar{s}\left(\left(\lambda_i + \psi_i\gamma_i\right)\dot{e}_i + \dot{\psi}_i\gamma_i e_i + \ddot{e}_i\right) + \frac{\dot{\mu}_i}{\rho_i}\left(\mu_i - \mu_i^*\right) + s_i\left(q_i(z) + v_i - \ddot{z}_{r_i} + \alpha_i\dot{\bar{z}}_i\right) \tag{25}$$

Substituting Eqs. (5), (12), (20), and (21) into (25) leads to

$$\begin{aligned}\dot{V}_i &= \bar{s}_i\left(-k_i\bar{s}_i\right) + s_i\left(q_i - \mu_i\text{sign}\left(s_i\right)\right) + |s_i|\left(\mu_i - \mu_i^*\right).\\ &= \bar{s}_i\left(-k_i\bar{s}_i\right) + |s_i|\left(Q_i - \mu_i\right) + |s_i|\left(\mu_i - \mu_i^*\right)\\ &= \bar{s}_i\left(-k_i\bar{s}_i\right) + |s_i|\left(Q_i - \mu_i^*\right).\end{aligned} \tag{26}$$

If the final value of the controller gain $\mu_i^*$ in (20) is large enough, i.e, $\mu_i^* > Q_i$, then we have a stable overall system, i.e $\dot{V}_i < 0$ and the system stability is guaranteed.

## IV. ENERGY CONSUMPTION

The method proposed in [37] is used to calculate the energy consumption of the feed drive system. The output power $P_i$ of a three phase AC motor is given by

$$P_i = \sqrt{3}P_{f_i}V_i\left(t\right)I_i\left(t\right), \tag{27}$$

whereby $V_i\left(t\right)$ and $I_i\left(t\right)$ are the instantaneous effective current and voltage of a motor, $P_{f_i}$ is the power factor for the $i^{th}$ axis. $P_{f_i}$ can be assumed to be constant when the load range of the motor is greater than a certain value. From (27), the energy consumption is given by

$$E_i = \sqrt{3}P_{f_i}\int_0^T V_i\left(t\right)\cdot I_i\left(t\right)dt, \tag{28}$$

$$I_i\left(t\right) = \frac{1}{K_{\mu_i}}\left[L_i\text{sign}(\dot{x}_i) + B_{e_i}\dot{x}_i\left(t\right) + J_{e_i}\ddot{x}_i\left(t\right)\right] \tag{29}$$

$$V_i\left(t\right) = I_i\left(t\right)Z_i + K_{E_i}\dot{x}_i\left(t\right), \tag{30}$$

where $Z_i$ is the impedance of the motor and $K_{E_i}$ is the back EMF coefficient. (28) - (30) lead to

$$E_i = \sqrt{3}P_{f_i}\int C_{1_i}\ddot{x}_i^2 + C_{2_i}\dot{x}_i^2 + C_{3_i}\dot{x}_i\text{sign}(\dot{x}_i) + C_{4_i} + C_{5_i}\ddot{x}_i\text{sign}(\dot{x}_i) + C_{6_i}\ddot{x}_i\dot{x}_i\,dt, \tag{31}$$

where

$$\begin{aligned}C_{1_i} &= J_{e_i}^2\frac{Z_i}{K_{\mu_i}^2}, \quad C_{2_i} = B_{e_i}\left(\frac{Z_iB_{e_i}}{K_{\mu_i}^2} + \frac{K_{E_i}}{K_{\mu_i}}\right),\\ C_{3_i} &= L_i\left(\frac{2Z_iB_{e_i}}{K_{\mu_i}^2} + \frac{K_{E_i}}{K_{\mu_i}}\right), \quad C_{4_i} = L_i^2\frac{Z_i}{K_{\mu_i}^2},\\ C_{5_i} &= 2L_iJ_{e_i}\frac{Z_i}{K_{\mu_i}^2}, \quad C_{6_i} = J_{e_i}\left(\frac{2Z_iB_{e_i}}{K_{\mu_i}^2} + \frac{K_{E_i}}{K_{\mu_i}}\right).\end{aligned}$$

(31) determines the energy only from the motion trajectory and constant.

## V. SIMULATION AND EXPERIMENT

To validate the effectiveness of the proposed method, simulation and experiment were conducted based on trajectories in Fig. 3 for $X_1$ and $X_2$ axis. Figure 4 shows the velocity profile for both $X_1$ and $X_2$ axes. The nonlinear second order plant in (3) is considered as the real system and the linear model in (6) was considered as the reference model. In simulation, an external disturbance of $d = [30, 30]^T$ N is applied to evaluate the performance in presence of matched uncertainty. The other plant and controller parameters are given in Tables 1 and 2 respectively. $k_i$ in Table 2 is a fixed gain for the SMC and an initial value for the adaptive gain $\hat{k}_i$. The same system parameters were used for both simulation and experiment.

**TABLE 1. System parameters.**

| Axis | $J_{e_i}$ (Ns$^2$/m) | $B_{e_i}$ (Ns/m) | $L_i$ (N) | $K_{\mu_i}$ (N/A) | $K_{E_i}$ (Vs/m) | $Z_i$ ($\Omega$) | $P_{f_i}$ |
|---|---|---|---|---|---|---|---|
| 1 | 88.08 | 467.20 | 45.50 | 124.76 | 140.00 | 10.00 | 0.43 |
| 2 | 97.90 | 631.00 | 54.80 | 200.22 | 200.00 | 15.00 | 0.45 |

**TABLE 2. Controller parameters.**

| Axis | $\lambda$ ($s^{-1}$) | $k_i$ ($s^{-1}$) | $\alpha$ ($s^{-1}$) | $\gamma$ ($s^{-1}$) | $\rho$ ($s^{-1}$) | $\beta$ | $\delta$ |
|---|---|---|---|---|---|---|---|
| 1 | 510 | 1000 | 10 | 1.5 | 3 | 5 | 0.1 |
| 2 | 510 | 1000 | 10 | 1.5 | 3 | 5 | 0.1 |

Comparison with the work in [25] was made to evaluate the performance. The previous work, referred as ASMC, is chosen for comparison because the sliding mode controller is robust and has been proven to provide satisfactory performance under the effect of external disturbances and system uncertainties. The new method includes the SMC based on the uncertainty dynamics and the ASMC. The following scenarios were considered:

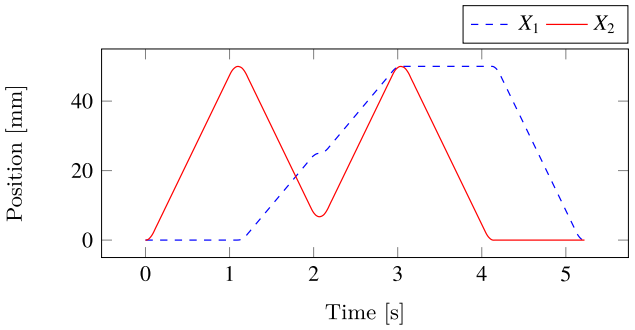


**FIGURE 3.** Reference positions.

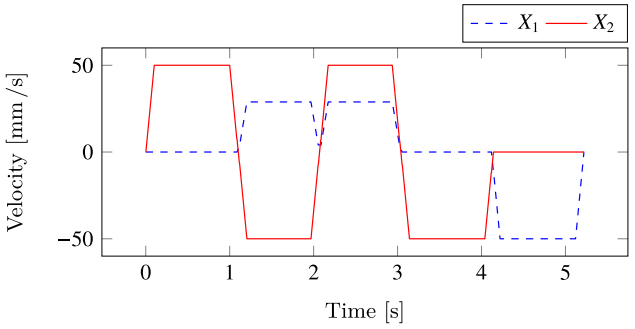


**FIGURE 4.** Reference velocities.

- Adaptive SMC (ASMC) only.
- Adaptive SMC with increased gain (ASMCIG).
- Adaptive SMC with uncertainty dynamics (ASMCU).
- SMC with uncertainty dynamics (SMCU)

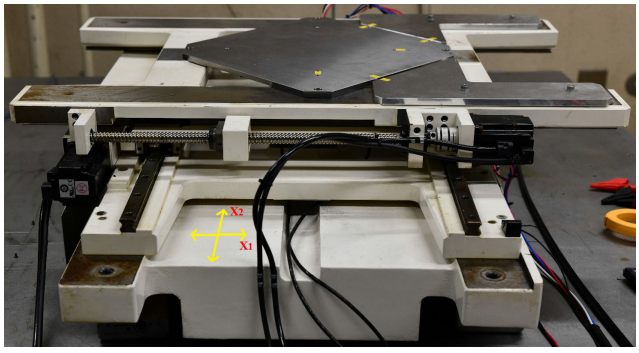


**FIGURE 5.** Industrial biaxial feed drive system.

### A. EXPERIMENTAL SETUP

An industrial biaxial ball-screw feed drive system (Fig. 5) was used for the experiment. The feed drive system comprises of a table coupled by two ball-screw drives, which are driven by AC-servo motors connected to each drive axis. Rotary encoders (equivalent resolution: 76.29 nm) were used to measure actual position of the table. The velocity signal was calculated by means of numerical differentiation of the measured position. The control law was implemented using

**TABLE 3.** Experimental controller parameters.

| Axis | $\lambda(s^{-1})$ | $\alpha(s^{-1})$ | $\gamma(s^{-1})$ | $\rho(s^{-1})$ | $\beta$ | $\delta$ |
|---|---|---|---|---|---|---|
| 1 | 1200 | 10 | 1.5 | 2 | 5 | 0.1 |
| 2 | 1200 | 10 | 1.5 | 2 | 5 | 0.1 |

C++ program on a personal computer with a sampling time of 0.2 ms.

### B. SIMULATION RESULTS

Figure. 6 shows simulation results of tracking performance in $X_1$ and $X_2$ axes. It can be seen that with the ASMC, the tracking error is larger in both axes compared to that of the ASMCU and SMCU. Also, the tracking performance of the ASMCU is slightly better than that of the SMCU. This is obvious because the adaptive part can automatically compensate for irregular changes within the control loop. Therefore, experimental analysis was conducted for the ASMC and ASMCU only. On the other hand, Fig. 7 shows that the control input signals of the ASMCU and SMCU are slightly larger than that of the ASMC. This is because the additional control input signals are generated by the the feedforward compensator in ASMCU and SMCU to compensate for the uncertainty dynamics. For clarity, summary of the simulation results are shown in Table 4.

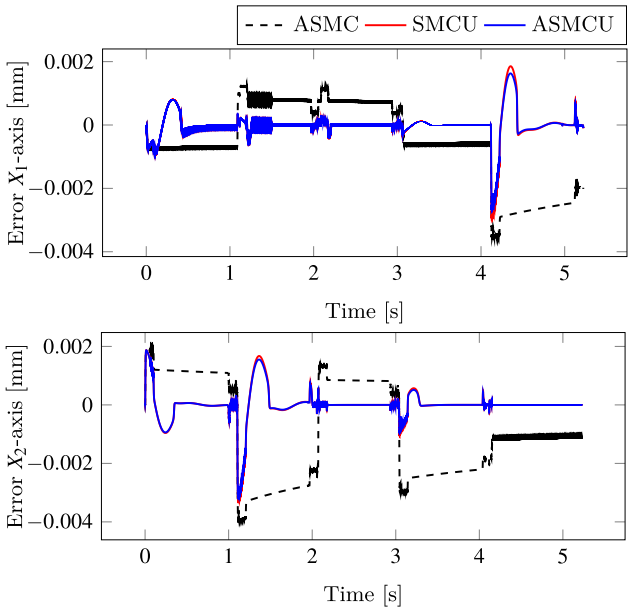


**FIGURE 6.** Simulation results of tracking error.

### C. EXPERIMENTAL RESULTS

An experiment was conducted on the trajectories in Fig. 3 for evaluating the tracking ability and energy saving performance for the proposed controller. The first aim was to confirm the effectiveness of the proposed method in tracking performance enhancement by comparing ASMC with the ASMCU. In this

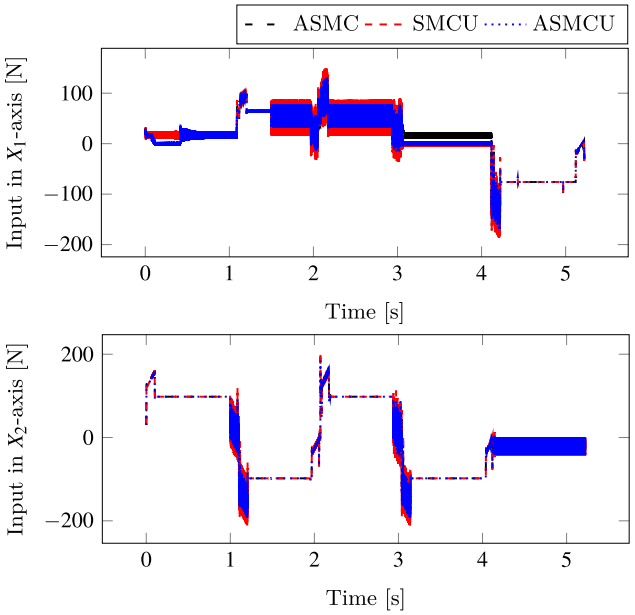


**FIGURE 7.** Simulation results of control input signal.

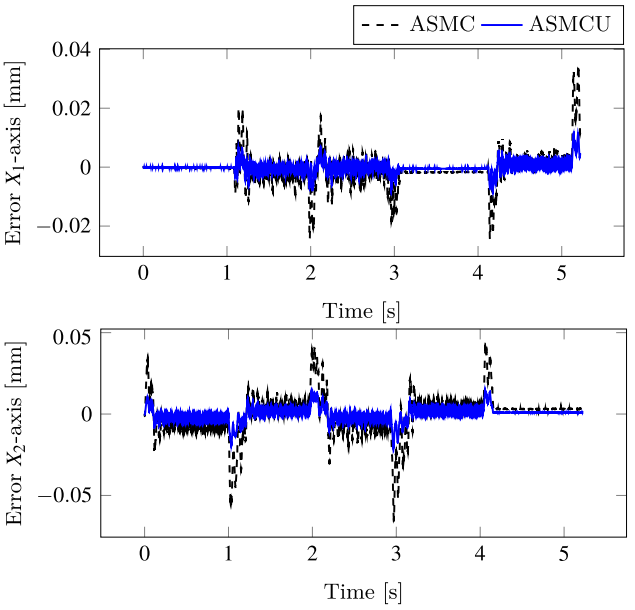


**FIGURE 8.** Experimental results of tracking error.

**TABLE 4.** Summary of simulation results.

| Controller | Tracking error [$\mu$m] | | | | Energy consumption [J] |
|---|---|---|---|---|---|
| | Maximum | | Average | | Total |
| | $X_1$-axis | $X_2$-axis | $X_1$-axis | $X_2$-axis | |
| ASMC | 2.50 | 2.68 | 0.77 | 1.13 | 20.9 |
| SMCU | 1.72 | 2.45 | 0.11 | 0.13 | 21.3 |
| ASMCU | 1.65 | 2.44 | 0.11 | 0.13 | 21.3 |

comparison, the same control parameters were applied for conducting a fare comparison as shown in Table 3. Furthermore, the same initial value of the adaptive gain $\hat{k}_i$ was applied on both controllers. The electrical energy consumption was measured and analyzed by the power analyzer (HIOKI 3390). For confirming the repeatability of the proposed controller, the same experiment was conducted five times. The absolute maximum tracking errors for all the trials are shown in Fig. 9, whereby the ASMCU attained smaller errors compared to the ASMC. Tracking error results for a single trial are shown in Fig. 8, which states that the ASMCU has better tracking performance over the ASMC. Using the ASMCU the average tracking error could be reduced by 33.33 %.

The control input signals are shown in Fig. 10 in which the control input signal of the ASMCU is slightly larger than that of the ASMC because the ASMCU generates additional control signal to compensate for the uncertainty dynamics. For the ASMC to achieve the similar tracking performance as the ASMCU, the linear term $\lambda_i$ of the sliding surface can be increased. However, it will result in high chattering of the input signal leading to higher energy consumption as confirmed later. Furthermore, the uncertainty states converge to zero as shown in Fig. 11. Fig. 12 shows the adaptation of the controller gain $\mu_i$, which was initialized as $\mu_i(0) = 0$

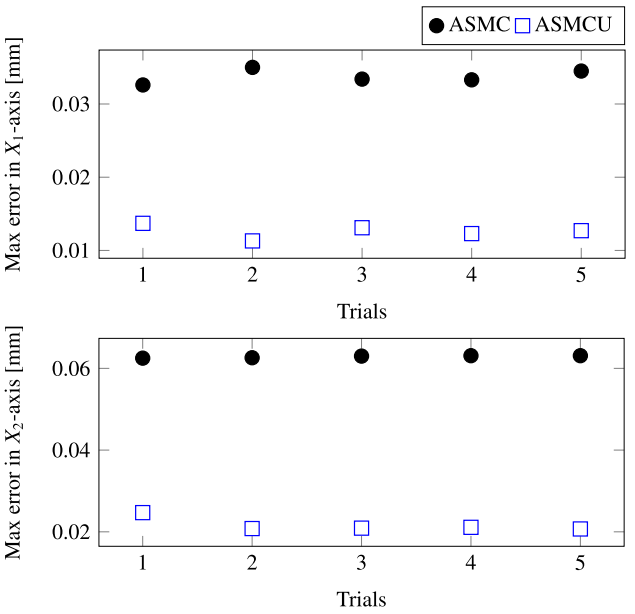


**FIGURE 9.** Experimental results of maximum tracking error.

**TABLE 5.** Summary of experimental results.

| Controller | Tracking error [mm] | | | | Energy consumption [J] |
|---|---|---|---|---|---|
| | Maximum | | Average | | Total |
| | $X_1$-axis | $X_2$-axis | $X_1$-axis | $X_2$-axis | |
| ASMC | 0.033 | 0.063 | 0.003 | 0.009 | 44.3 |
| ASMCIG | 0.015 | 0.024 | 0.08 | 0.09 | 45.9 |
| ASMCU | 0.013 | 0.021 | 0.001 | 0.007 | 44.9 |

for both axes. Due to the adaptation rule, the gains were able to reach large final values which make the system stable.

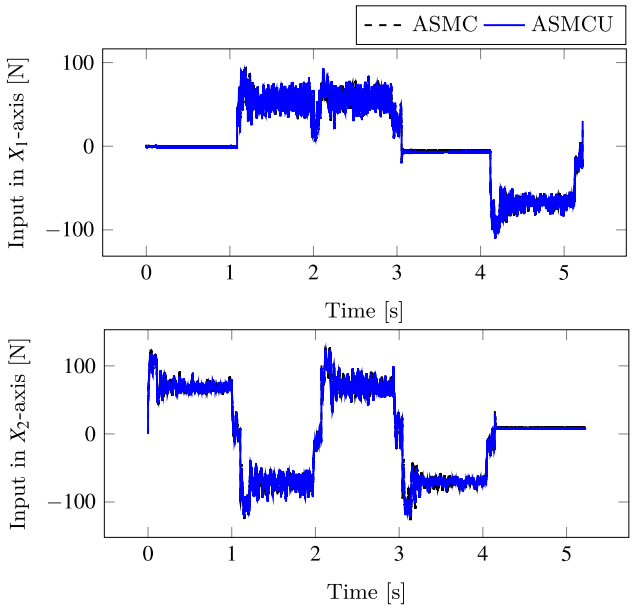


**FIGURE 10.** Control input signal.

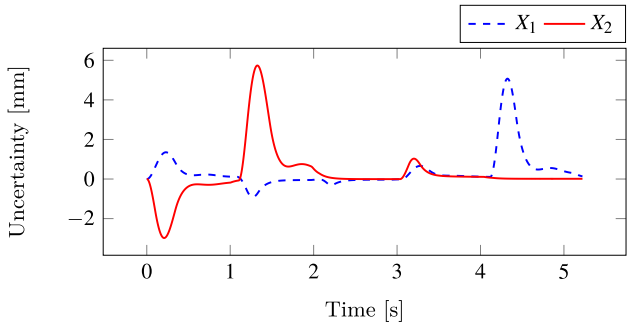


**FIGURE 11.** Uncertainty state.

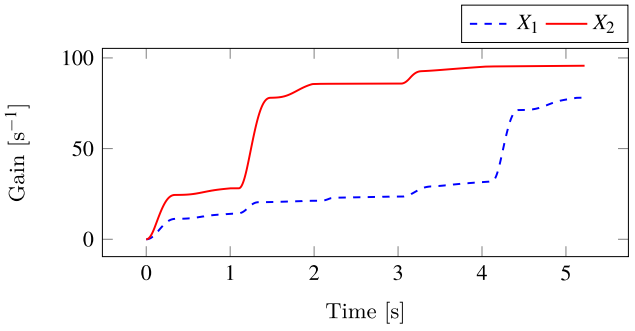


**FIGURE 12.** Controller gain $\mu$.

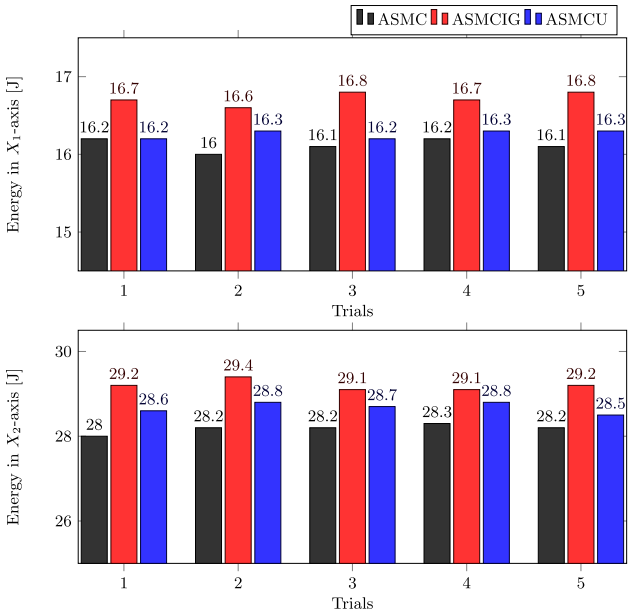


**FIGURE 13.** Energy consumption.

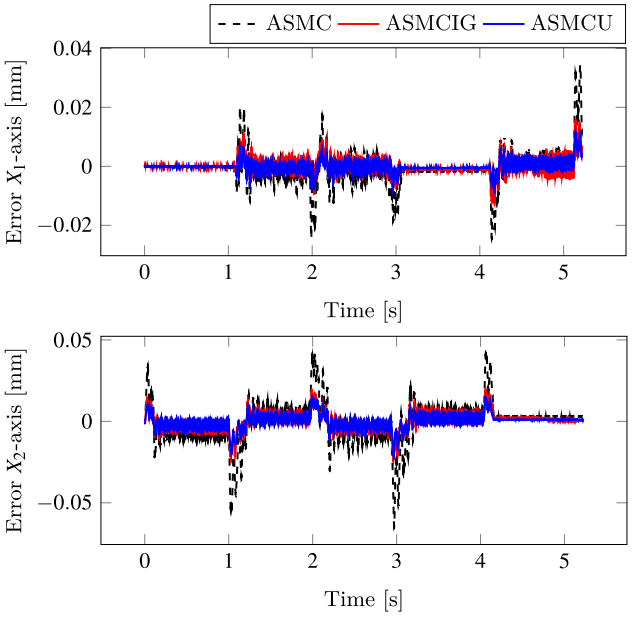


**FIGURE 14.** Experimental results of tracking error under similar tracking performance.

Next, we confirm the effectiveness of the proposed method in saving energy under the similar tracking performance. To achieve the similar tracking performance for both ASMC and the proposed method, the linear term $\lambda_i$ of the sliding surface was increased from $1200\,s^{-1}$ to $2000\,s^{-1}$. Fig. 13 shows the experimental results of energy consumption for five trials in which the ASMCIG consumed more energy than the ASMC and the ASMCU for all trials. This is because without a compensator, in order to achieve good tracking performance, disturbances are handled by applying high gains in the controller which increase control input variance due to noise causing higher energy consumption. On the other hand, when the compensator is used, high gains are unnecessary in the controller because the disturbances are handled by the compensator and therefore less energy consumption. With the raised linear-term gain, the total energy consumed by the ASMCIG increased from 44.3 J to 45.9 J on average

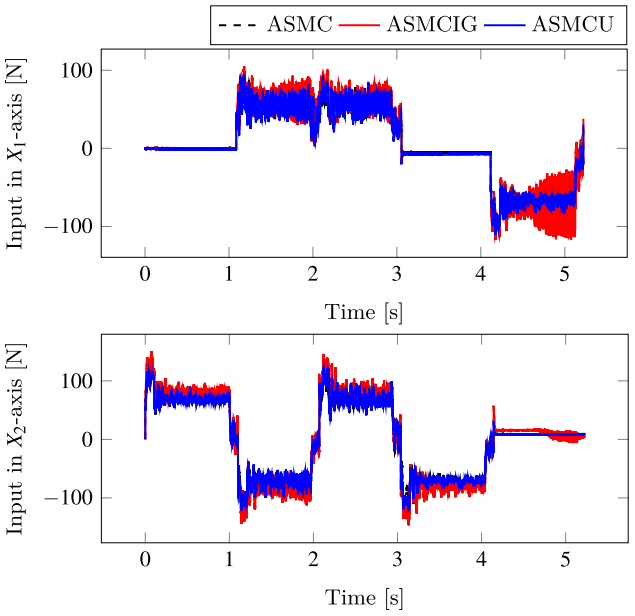


**FIGURE 15.** Control input signal under similar tracking performance.

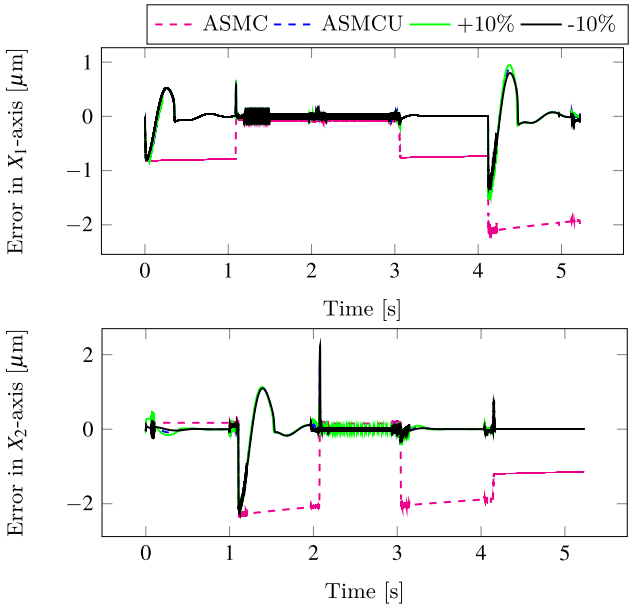


**FIGURE 16.** Simulation results under changing parameters ($J_e$ and $B_e$ are changed by 10 %).

as in Table 5. Fig. 14 shows the tracking performance for the three cases, case one for the same parameters, case two with increased $\lambda_i$ (ASMCIG), and case three is the ASMCU. Fig. 15 shows the corresponding input signals, where the control input for ASMCIG has more chattering compared to others. The control input standard deviation for ASMCIG increased from 55.00 to 62.97 N in comparison to the ASMC. The proposed method achieved input standard deviation of 55.03V.

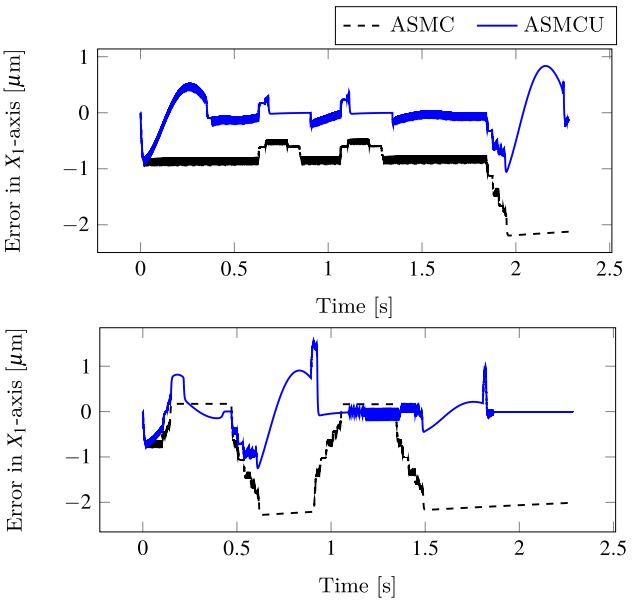


**FIGURE 17.** Simulation results under high speed (200mm/s).

## VI. DISCUSSION

Figure 16 shows simulation results of tracking performance in $X_1$ and $X_2$ axes when parameters change. We changed the values of $J_e$ and $B_e$ by 10 % and checked the tracking performance of the proposed controller. With these results, we can conclude that the proposed controller can still achieve good performance. Figure 17 shows simulation results of tracking performance in $X_1$ and $X_2$ axes when considering high speed of 200mm/s. It can be seen that with the ASMC, the tracking error is larger in both axes compared to that of the ASMCU. Using the ASMCU the average tracking error could be reduced by 67.9 %, while the absolute maximum tracking error could be reduced by 35.5 %. Therefore, we conclude that the proposed controller can be used to increase tracking performance in feed drive systems with higher speeds. As future works, it is interesting to consider including LuGre friction model in the compensation strategy and consider improving contouring performance.

## VII. CONCLUSION

This study proposes an adaptive sliding mode control with a nonlinear sliding surface and a model-based feedforward compensator for uncertainty dynamics for application in feed drive systems. Its effectiveness was evaluated by both simulation and experimental analyses. Experimental results revealed that, as compared to the adaptive sliding mode controller, the proposed controller could achieve a substantial tracking performance, whereby the average tracking error could be reduced by 33.33 % and the maximum tracking error by about 64 % on average. In addition, the energy consumption could be reduced by 2 % on average under similar tracking performance. Because a typical bi-axial feed drive system

was considered in this study, authors believe that the proposed controller can be applied to any configuration of feed drive systems.

## REFERENCES

[1] X. Xu, G.-Y. Gu, Z. Xiong, X. Sheng, and X. Zhu, "Development of a decentralized multi-axis synchronous control approach for real-time networks," *ISA Trans.*, vol. 68, pp. 116–126, May 2017. [Online]. Available: http://www.sciencedirect.com/science/article/pii/S0019057817303518

[2] B. Zhu and R. T. Farouki, "A general framework for solving inverse dynamics problems in multi-axis motion control," *ISA Trans.*, vol. 95, pp. 130–143, Dec. 2019. [Online]. Available: http://www.sciencedirect.com/science/article/pii/S0019057819302344

[3] K. R. Simba, B. D. Bui, M. R. Msukwa, and N. Uchiyama, "Robust iterative learning contouring controller with disturbance observer for machine tool feed drives," *ISA Trans.*, vol. 75, pp. 207–215, Apr. 2018.

[4] C.-H. Wu and Y.-T. Kung, "Thermal analysis for the feed drive system of a CNC machine center," *Int. J. Mach. Tools Manuf.*, vol. 43, no. 15, pp. 1521–1528, Dec. 2003. [Online]. Available: http://www.sciencedirect.com/science/article/pii/S0890695503002207

[5] Y. Altintas, A. Verl, C. Brecher, L. Uriarte, and G. Pritschow, "Machine tool feed drives," *CIRP Ann.*, vol. 60, no. 2, pp. 779–796, 2011.

[6] L. Dong and W. C. Tang, "Adaptive backstepping sliding mode control of flexible ball screw drives with time-varying parametric uncertainties and disturbances," *ISA Trans.*, vol. 53, no. 1, pp. 110–116, Jan. 2014.

[7] J. Uk Cho, Q. Ngoc Le, and J. Wook Jeon, "An FPGA-based multiple-axis motion control chip," *IEEE Trans. Ind. Electron.*, vol. 56, no. 3, pp. 856–870, Mar. 2009.

[8] P. Li and G. Zhu, "Robust internal model control of servo motor based on sliding mode control approach," *ISA Trans.*, vol. 93, pp. 199–208, Oct. 2019. [Online]. Available: http://www.sciencedirect.com/science/article/pii/S001905781930151X

[9] Y. Xie, X. Tang, B. Song, X. Zhou, and Y. Guo, "Data-driven adaptive fractional order PI control for PMSM servo system with measurement noise and data dropouts," *ISA Trans.*, vol. 75, pp. 172–188, Apr. 2018. [Online]. Available: http://www.sciencedirect.com/science/article/pii/S0019057818300776

[10] W. Zhang, N. Nan, Y. Yang, W. Zhong, and Y. Chen, "Force ripple compensation in a PMLSM position servo system using periodic adaptive learning control," *ISA Trans.*, vol. 95, pp. 266–277, Dec. 2019. [Online]. Available: http://www.sciencedirect.com/science/article/pii/S001905781930206X

[11] J. Yao, G. Yang, Z. Jiao, and D. Ma, "Adaptive robust motion control of direct-drive DC motors with continuous friction compensation," *Abstract Appl. Anal.*, vol. 2013, pp. 1–14, 2013.

[12] W. Deng and J. Yao, "Adaptive integral robust control and application to electromechanical servo systems," *ISA Trans.*, vol. 67, pp. 256–265, Mar. 2017. [Online]. Available: http://www.sciencedirect.com/science/article/pii/S0019057817301581

[13] S. Wang, J. Na, H. Yu, and Q. Chen, "Finite time parameter estimation-based adaptive predefined performance control for servo mechanisms," *ISA Trans.*, vol. 87, pp. 174–186, Apr. 2019. [Online]. Available: http://www.sciencedirect.com/science/article/pii/S0019057818304713

[14] S.-Y. Chen, T.-H. Li, and C.-H. Chang, "Intelligent fractional-order backstepping control for an ironless linear synchronous motor with uncertain nonlinear dynamics," *ISA Trans.*, vol. 89, pp. 218–232, Jun. 2019. [Online]. Available: http://www.sciencedirect.com/science/article/pii/S0019057818305317

[15] J. Yao, Z. Jiao, and D. Ma, "RISE-based precision motion control of DC motors with continuous friction compensation," *IEEE Trans. Ind. Electron.*, vol. 61, no. 12, pp. 7067–7075, Dec. 2014.

[16] C. Li, C. Li, Z. Chen, and B. Yao, "Advanced synchronization control of a dual-linear-motor-driven gantry with rotational dynamics," *IEEE Trans. Ind. Electron.*, vol. 65, no. 9, pp. 7526–7535, Sep. 2018.

[17] Z. Chen, C. Li, B. Yao, M. Yuan, and C. Yang, "Integrated coordinated/synchronized contouring control of a dual-linear-motor-driven gantry," *IEEE Trans. Ind. Electron.*, vol. 67, no. 5, pp. 3944–3954, May 2020.

[18] J. Zheng, H. Wang, Z. Man, J. Jin, and M. Fu, "Robust motion control of a linear motor Positioner using fast nonsingular terminal sliding mode," *IEEE/ASME Trans. Mechatronics*, vol. 20, no. 4, pp. 1743–1752, Aug. 2015.

[19] X. Li, H. Zhao, X. Zhao, and H. Ding, "Dual sliding mode contouring control with high accuracy contour error estimation for five-axis CNC machine tools," *Int. J. Mach. Tools Manuf.*, vol. 108, pp. 74–82, Sep. 2016.

[20] X.-C. Xi, W.-S. Zhao, and A.-N. Poo, "Improving CNC contouring accuracy by robust digital integral sliding mode control," *Int. J. Mach. Tools Manuf.*, vol. 88, pp. 51–61, Jan. 2015.

[21] J. Yang and Y. Altintas, "A generalized on-line estimation and control of five-axis contouring errors of CNC machine tools," *Int. J. Mach. Tools Manuf.*, vol. 88, pp. 9–23, Jan. 2015.

[22] A. M. Abd El Khalick Mohammad, N. Uchiyama, and S. Sano, "Energy saving in feed drive systems using Sliding-Mode-Based contouring control with a nonlinear sliding surface," *IEEE/ASME Trans. Mechatronics*, vol. 20, no. 2, pp. 572–579, Apr. 2015.

[23] R. Raman, A. Chalanga, S. Kamal, and B. Bandyopadhyay, "Nonlinear sliding surface based adaptive sliding mode control for industrial emulator," in *Proc. IEEE Int. Conf. Ind. Technol. (ICIT)*, Feb. 2013, pp. 124–129.

[24] M. R. Msukwa, N. Uchiyama, and B. Dinh Bui, "Adaptive nonlinear sliding mode control with a nonlinear sliding surface for feed drive systems," in *Proc. IEEE Int. Conf. Ind. Technol. (ICIT)*, Mar. 2017, pp. 732–737.

[25] M. R. Msukwa and N. Uchiyama, "Design and experimental verification of adaptive sliding mode control for precision motion and energy saving in feed drive systems," *IEEE Access*, vol. 7, pp. 20178–20186, 2019.

[26] A. T. Elfizy, G. M. Bone, and M. A. Elbestawi, "Model-based controller design for machine tool direct feed drives," *Int. J. Mach. Tools Manuf.*, vol. 44, no. 5, pp. 465–477, Apr. 2004. [Online]. Available: http://www.sciencedirect.com/science/article/pii/S0890695503003110

[27] A. Kamalzadeh, D. J. Gordon, and K. Erkorkmaz, "Robust compensation of elastic deformations in ball screw drives," *Int. J. Mach. Tools Manuf.*, vol. 50, no. 6, pp. 559–574, Jun. 2010. [Online]. Available: http://www.sciencedirect.com/science/article/pii/S0890695510000337

[28] J. Yao, W. Deng, and Z. Jiao, "Adaptive control of hydraulic actuators with LuGre model-based friction compensation," *IEEE Trans. Ind. Electron.*, vol. 62, no. 10, pp. 6469–6477, Oct. 2015.

[29] A. Verl and S. Frey, "Correlation between feed velocity and preloading in ball screw drives," *CIRP Ann.*, vol. 59, no. 1, pp. 429–432, 2010. [Online]. Available: http://www.sciencedirect.com/science/article/pii/S000785061000137X

[30] S. Yamada, H. Fujimoto, and Y. Terada, "Joint torque control for backlash compensation in two-inertia system," in *Proc. IEEE 25th Int. Symp. Ind. Electron. (ISIE)*, Jun. 2016, pp. 1138–1143.

[31] E. Kayacan and J. Peschel, "Robust model predictive control of systems by modeling mismatched uncertainty," *IFAC-PapersOnLine*, vol. 49, no. 18, pp. 265–269, 2016.

[32] D. Prevost, S. Lavernhe, C. Lartigue, and D. Dumur, "Feed drive modelling for the simulation of tool path tracking in multi-axis high speed machining," *Int. J. Mechatronics Manuf. Syst.*, vol. 4, nos. 3–4, pp. 266–284, 2011.

[33] B. Bandyopadhyay, F. Deepak, and K. S. Kim, *Sliding Mode Control Using Novel Sliding Surfaces*, vol. 392. Berlin, Germany: Springer-Verlag, 2009.

[34] A. E. K. Mohammad, N. Uchiyama, and S. Sano, "Reduction of electrical energy consumed by feed-drive systems using sliding-mode control with a nonlinear sliding surface," *IEEE Trans. Ind. Electron.*, vol. 61, no. 6, pp. 2875–2882, Jun. 2014.

[35] Y. X. Su, D. Sun, and B. Y. Duan, "Design of an enhanced nonlinear PID controller," *Mechatronics*, vol. 15, no. 8, pp. 1005–1024, Oct. 2005.

[36] F. Plestan, Y. Shtessel, V. Brégeault, and A. Poznyak, "New methodologies for adaptive sliding mode control," *Int. J. Control*, vol. 83, no. 9, pp. 1907–1919, Sep. 2010.

[37] N. Uchiyama, K. Goto, and S. Sano, "Analysis of energy consumption in fundamental motion of industrial machines and experimental verification," in *Proc. Amer. Control Conf. (ACC)*, Jul. 2015, pp. 2179–2184.

**MATHEW RENNY MSUKWA** (Student Member, IEEE) received the B.Sc. degree in electromechanical engineering from the University of Dar es Salaam, Tanzania, in 2013, and the M.Eng. degree from the Toyohashi University of Technology, Japan, in 2017, where he is currently pursuing the Ph.D. degree. Since 2013, he has been with the Department of Electrical Engineering, University of Dar es Salaam, where he is also an Assistant Lecturer. His research interests are machine tool control, industrial robotics, and mechatronics systems design and control. He is a Student Member of IEEE IES.

**ENOCK WILLIAM NSHAMA** received the B.Sc. degree in electromechanical engineering from the University of Dar es Salaam, Tanzania, in 2014, and the M.Eng. degree from the Toyohashi University of Technology, Japan, in 2018, where he is currently pursuing the Ph.D. degree. Since 2016, he has been with the Department of Mechanical Engineering, University of Dar es Salaam, where he is also an Assistant Lecturer. His research interests are machine tool control, industrial robotics, and mechatronics systems design and control.

**NAOKI UCHIYAMA** (Member, IEEE) received the B.E. degree from the Numazu National College of Technology, Shizuoka, Japan, in 1988, the B.E. and M.E. degrees from Shizuoka University, Shizuoka, in 1990 and 1992, respectively, and the Ph.D. degree in mechanical engineering from Tokyo Metropolitan University, Tokyo, Japan, in 1995. He was a Visiting Scholar with the University of California, Davis, from 2001 to 2002. Since 1995, he has been with the Department of Mechanical Engineering, Toyohashi University of Technology, Japan, where he is currently a Professor. He is a member of IEEE IES, CSS, and RAS.